Three-Dimensional Shock-Wave/Boundary-Layer Interaction at the Presence of Entropy Layer

V. Borovoy, I. Egorov, V. Mosharov, V. Radchenko, A. Skuratov, I. Struminskaya, A. Volkova

Central Aerohydrodynamic Institute (TsAGI)

140180 Zhukovsky, Moscow Region, Russia

Abstract

Experimental and numerical investigation of gas flow on a flat plate near a single fin and a fin pair, generating crossings shocks, is performed. The study is focused upon the plate bluntness influence on the flow field and heat transfer in the interaction region. The experiments are carried out in the short duration wind tunnel at Mach numbers M=5, 6 and 8 and Reynolds numbers $Re_{\infty L}$ up to $27x10^6$. Luminescent substances are applied for measurements of heat flux and pressure and for surface flow visualization. In addition, heat flux is measured by thermocouple sensors. For numerical flow simulation, the three-dimensional Reynolds-averaged Navier-Stokes equations are solved, using the q-ω turbulence model.

It is established that even small plate blunting significantly influences on heat transfer and pressure distributions. Moreover in some cases, it can cause global transformation of the flow structure in the area of interference between the shock waves and boundary layer.

1. Introduction

A great number of works (for-example [1-8]) are dedicated to the investigation of interaction of the oblique shock waves, generated by a single fin or a fin pair, with boundary layer of the plate on which they are installed. Firstly, experimental investigations were carried out. During last two decades, high attention has been also paid to the numerical simulation of such flows. The review of the experimental and computational works performed up to 2003 is presented in [7].

Almost in all the works, the interference flow on the sharp plate is studied. At the same time, the investigations of two-dimensional interference between an oblique shock wave and laminar boundary layer of the plate [9-11] show that even a small bluntness of the plate leading edge significantly decreases heat exchange in the shock incidence region. It also turns out that there is a threshold value of the plate blunting radius [10]: the maximum heat transfer coefficient significantly decreases as the radius increases only up to a certain threshold value; the further blunting slightly influences on the maximum value of the heat-transfer coefficient. These peculiarities are related to the influence of the high-entropy layer, generated by the blunted leading edge, on the flow in the separation zone, caused by the incident shock wave.

The influence of a small blunting on the gas flow and heat exchange in the region of interaction between a single fin and the plate at Mach number M = 6 and Reynolds numbers $Re_{\infty L}$ up to $19.2x10^6$ is investigated in [12]. The undisturbed boundary layer ahead the fin was laminar or transitional. It is shown that at laminar boundary layer in front of the fin, the maximum Stanton number behind the shock reaches approximately the same value as in the case of turbulent flow or even exceeds this level. Small blunting of the plate leading edge leads to significant decrease of the maximum Stanton number and to certain expansion of the region of amplified heat transfer. The decrease of heat transfer, caused by the plate blunting, occurs only in a limited range of the blunting radius (at $r/X_o \leq 0.02$-0.03). At $r/X_o \geq 0.03$, the blunting influence is negligible.

In the present work, interaction of shock waves with turbulent boundary layer (at M=5 and 6) and laminar boundary layer (at M=8) is investigated. The flow in the vicinity of a single fin and a fin pair, generating crossing shocks, is studied. In the second case, the degree of the channel contraction, which is formed between the fins, is varied.

2. Models. Flow characteristics.

The main part of the models is the plate 1 (Fig. 1). Three variants of the plate are used. 1) The steel plate is destined for measuring the heat transfer coefficient by the “thin wall” sensors. The sensors are situated in three sections (Fig. 1): at the symmetry line and in two cross-sections. 2) Similar steel plate with the heat insulating coating made of glass-reinforced plastic. It is destined for measuring the heat transfer coefficient using TSP. 3) The plate made of an aluminum alloy. It is destined for measuring pressure distribution using PSP and surface flow visualization by the oil, containing solid fluorescent particles.

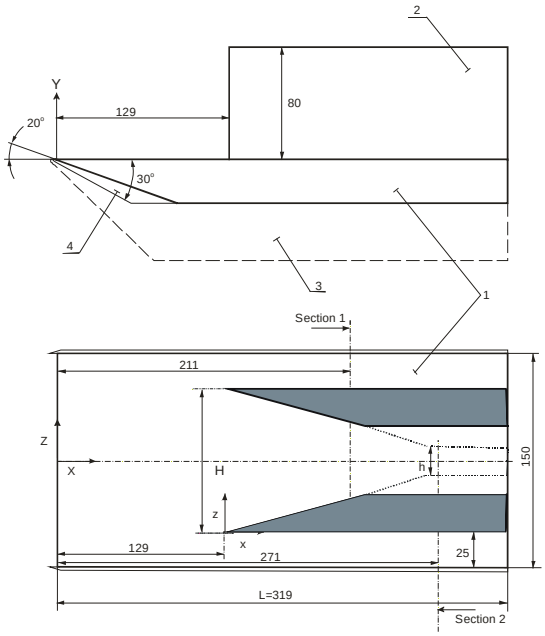

Figure 1: Test configuration and coordinate systems

One fin or two asymmetric fins are installed on the plate at the distance 129 mm from its leading edge. All the fins are sharp. Single fins with flow deflection angles $\theta = 10^o$, 15^o and 20^o are tested. In the case of the fin pair, the fins with $\theta = 15^o$ are used only. At that, the fin thickness is varied so that the contraction ratio of the channel, formed between the fins, is 0.5 or 0.25. On the plate, the replaceable front pad 4 is fixed. It is used for variation of the plate bluntness. In addition, the longitudinal fences 3, reducing the gas flow from one plate surface to the other, are installed on the plate.

The experiments are carried out in the TsAGI shock wind tunnel UT-1M. It operates according to the Ludwieg tube scheme. Duration of the stationary flow is 40 msec. The characteristics of the undisturbed flow are presented in the table.

Table 1. Flow characteristics

Mach number M	Total pressure P_t, bar	Total temperature T_t, K	Reynolds number $Re_{\infty L}$(L=0.32m)
5	69	530	$27x10^6$
6	90	560	$19x10^6$
8	90	690	$7x10^6$

At Mach number M=5, natural laminar/turbulent transition takes place on the plate ahead the fins. At M=6, trip is used for boundary layer turbulization near the plate leading edge. At M=8, the undisturbed boundary layer was laminar.

3. Investigation methods

The distributions of heat transfer and pressure are investigated by the help of luminescent thermal sensitive paint (TSP) and pressure sensitive paint (PSP). The measurement methods are described in details earlier [12, 13]. In the present work, the modifications allowing simultaneously observation of the entire plate surface are introduced into the technology of the TSP and PSP applications. Together with the optical (panoramic) methods, discrete measurements of heat flux using the "thin wall" sensors are applied.

For visualization of surface flow and skin friction, the method recently developed in TsAGI is applied [13]. Small displacements of the luminescent particles introduced in the oil are measured.

For numerical flow simulation, the three-dimensional Reynolds-averaged Navier-Stokes equations are solved, using the q-ω turbulence model [11].

4. Single fin on the plate.

4.1 Flow pattern

At a sufficiently high intensity of the shock generated by the fin, boundary layer separates from the plate surface. The separation zone can be divided into two parts [2, 4]: the initial region and the region of developed separation. The length of the initial region is (10-12)δ at the laminar state of the undisturbed boundary layer (δ is its thickness) and (6-8)δ at the turbulent state [2]. In the initial region, the flow characteristics significantly vary both along the fin and in the perpendicular direction. In the second region, the flow parameters slightly vary along the rays originating at the virtual pole, situated in front of the fin. This region is specified as a quasi-conical region [3, 8]. The majority of works focus upon the second region. However, the length of the first region can constitute a significant part of the fin length or even cover the entire fin. The length of the initial region increases with displacing the fin from the plate leading edge (with boundary-layer thickening). This investigation shows that increase of the plate bluntness and Mach number also elongates the first region.

At the 2D separation flow, a closed separation zone forms (Fig. 2a [3]). At that, the dividing streamline separated from the plate surface (at the point S_1) reattaches to it (at the point R_1). In the vicinity of the point R_1, heat flux and pressure dramatically increase.

.

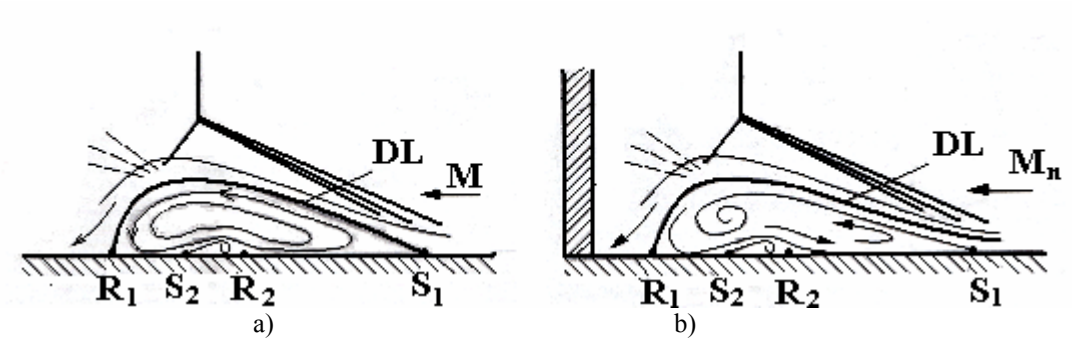

Figure 2: Flow patterns: a) 2D separation flow, b) 3D separation flow

At the 3D separation flow near a sharp fin, the separation zone expands with the distance from the fin leading edge. Therefore, inviscid gas inflows continuously into the separation zone, and the boundary of the separation zone is not closed (Fig. 2b): the streamline, separated at the point S_1, does not reattach to the surface; it moves downstream in a spiral form, and another streamline, displaced from the plate surface (on the distance Y_s), attaches to the plate. Such separation flow pattern near a fin is confirmed by numerical flow simulation in [4].

In the initial region, the attaching stream lines are characterized by low values of total pressure P_o and stagnation temperature T_o. Firstly, this is because they emanated at small distance Y_s from the plate surface. Secondary, due to small lateral dimension of the separation zone, the separated jet dos not have sufficient time to increase significantly the values P_o and To. The heat transfer and pressure coefficients on the reattachment line gradually increase with the distance from the fin leading edge.

At a great distance from the fin leading edge (in the region of a quasi-conical flow), where the gas jet emanated from the external part of the boundary layer (or inviscid gas) attaches to the plate, parameters P_o and T_o approach their values in the external flow (in the case of a sharp plate) or in the high-entropy layer (in the case of a strongly blunted plate). At further distancing from the fin leading edge, the parameters P_o and To vary slightly.

Small blunting of the plate provokes decrease of the heat transfer and pressure coefficients on the reattachment line. This occurs because the gas density in the mixing layer reduces and its thickness increases due to the admixture of less density gas from the high-entropy layer. At high bluntness, the gas density on the external boundary of the mixing layer is determined by the characteristics of the high-entropy layer. At that, the thickness of high-entropy layer practically do not influences the characteristics of the mixing layer, and the further blunting increase slightly influences the heat transfer and pressure on the reattachment line. However, the bluntness increase causes thickening of the high-entropy layer. The involvement of this layer into the separation flow leads to expansion of the separation zone.

The presented below experimental and computational data specify the flow characteristics in the region of interaction between a fin and a fin pair with the plate.

4.2 Distributions of heat-transfer and pressure coefficients in the interference zone

The distributions of Stanton number St, pressure coefficient Cp and limiting streamlines over the surface of sharp (r=0) and blunted (r=0.75 mm) plates with the fin $\theta = 15^o$ are presented in Fig. 3. It is evident that the separation zone is formed near the fin. Stanton number, surface pressure and skin friction (the skin friction is displayed by color) sharply increase on the reattachment line (near the fin). Comparison of data for the sharp and blunted plates shows that the plate blunting leads to the reduction of heat transfer, pressure and friction. Simultaneously, the region influenced by the fin expands.

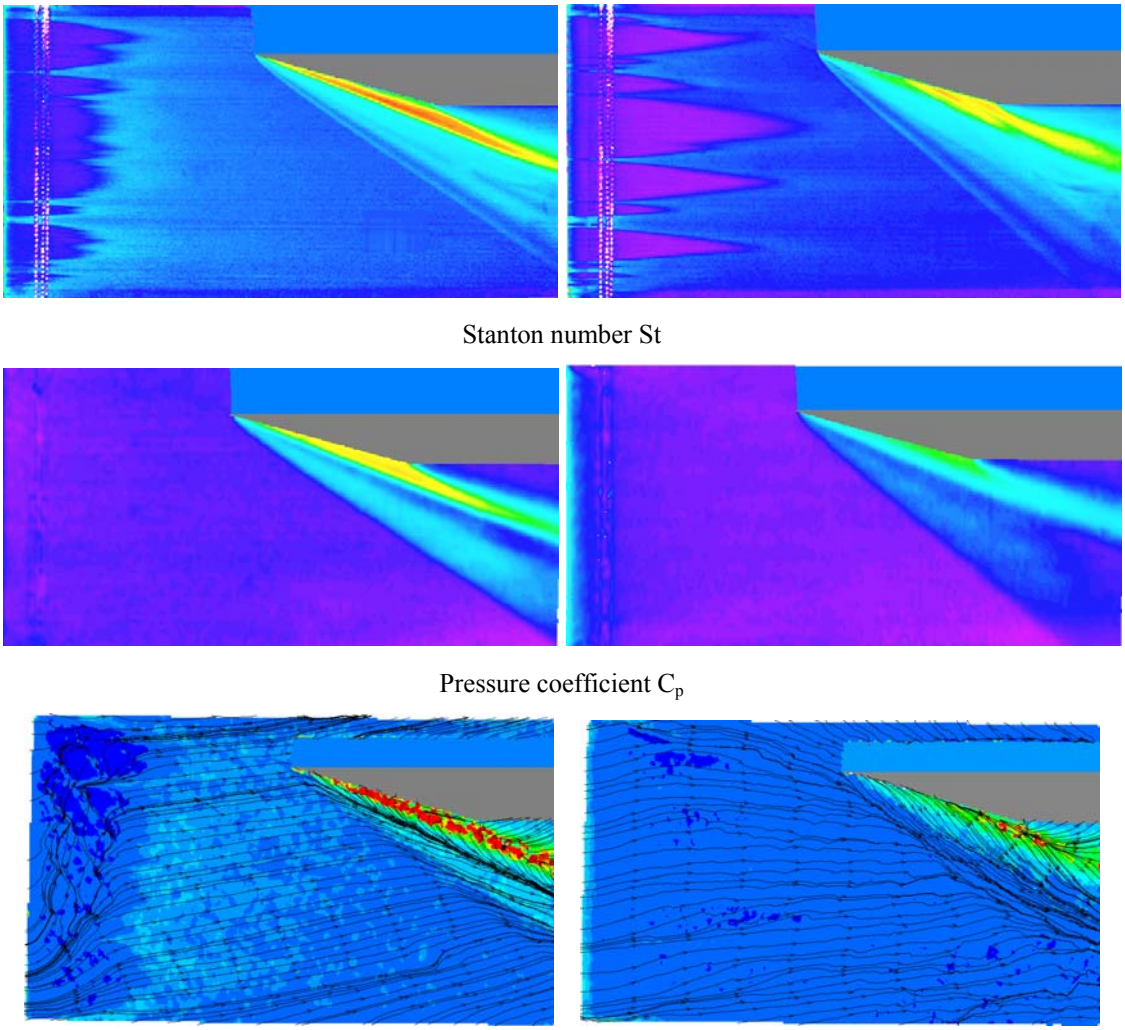

Stanton number St

Pressure coefficient C_p

Limiting stream lines and skin friction

Figure 3: Flow fields on the sharp and blunted plates at M = 5 and $\theta = 15^o$: left – sharp plate (r =0), right – blunted plate (r = 0.75 mm, $r/X_o = 5.8x10^{-3}$)

It is also seen from Fig. 3 that the heat transfer and pressure coefficients gradually increase at the distancing from the fin leading edge along the reattachment line. Fig. 4 provides with the quantitative information on this fact. The

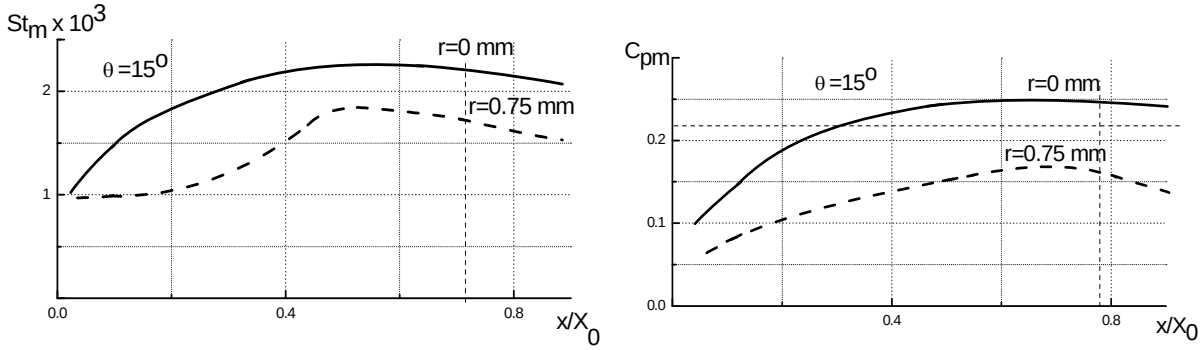

Figure 4: Longitudinal distributions of Stanton number and pressure coefficient on the dividing line at M=5 and

θ =15°. Vertical dashed line – angular point on the fin, horizontal dashed line – Cp, calculated for the non viscous flow

tendency to the elongation of the initial zone at reduction of the fin angle θ is observed: at θ=10° the initial zone is significantly longer than at θ=15°. The plate leading edge blunting also elongates the initial region of interference.

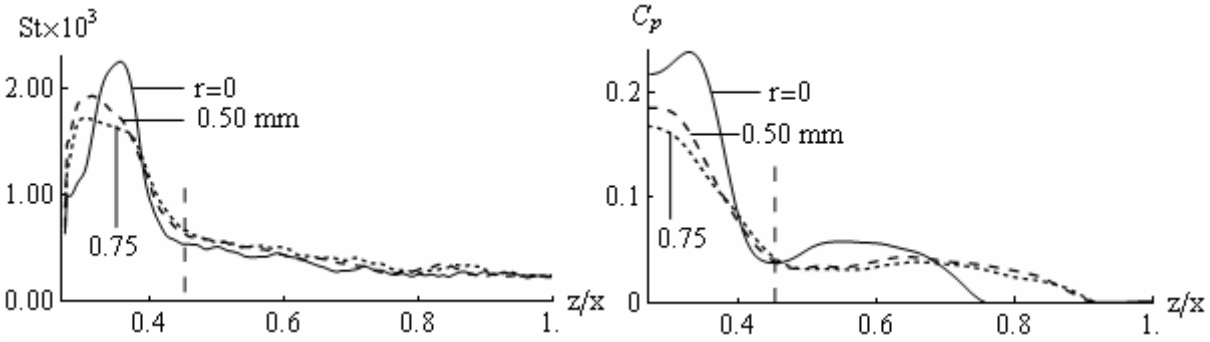

Figure 5: Lateral distributions of Stanton number and pressure coefficient in the cross section $x/X_o = 0.64$ at M=5 and θ =15°.

For example, at θ=10° the increase in the plate bluntness radius from r =0 up to r=0.75 mm almost doubles the length of the initial region. At θ=20°, the initial region of interference occupies the entire length of the fin (up to the angular point) even on the sharp plate (however, the fin length at θ=20° is shorter than at θ=10° и 15°, because all the fins used in optical measurements have the same thickness b = 25 mm).

The lateral distributions of the heat transfer and pressure coefficients near the fin θ=15° in the cross section x/X_o = 0.64, which is situated in the region of a quasi-cone flow, are presented in Fig. 5. It is seen that two maxima of pressure are formed: the absolute maximum is located behind the shock wave, on the line of primary reattachment, and the local maximum is located on the reattachment line behind the secondary separation. In the Stanton number distribution, the absolute maximum of the Stanton number is seen too, but the local maximum is undistinguished here. This can be explained by an insufficient distance between the section x/X_o = 0.64 and the fin leading edge. Both the local minimum and local maximum of heat flux can be seen in Fig. 3 at a greater distance from the fin leading edge (behind the angular point).

4.3 Influence of the plate bluntness on the maximum values of heat transfer and pressure coefficients

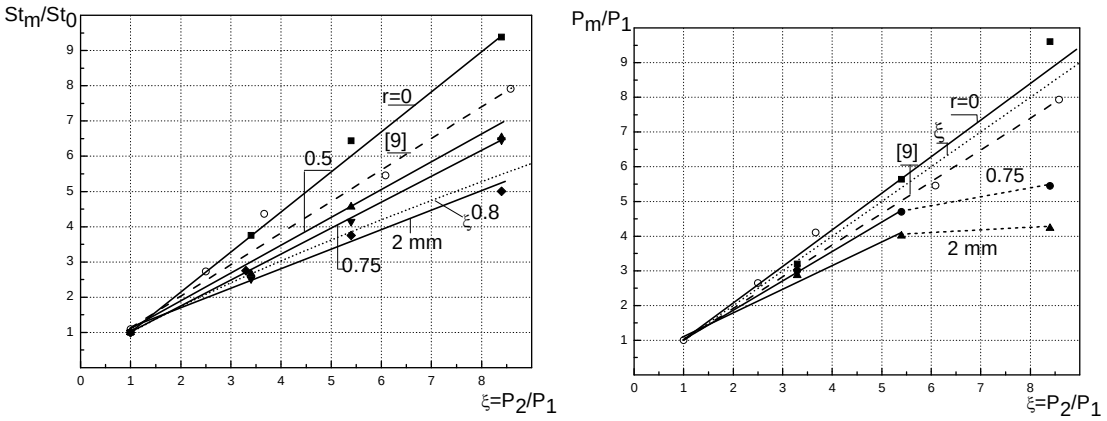

Figure 6: Maximum heat transfer amplification St_m/St_o and maximum pressure increase P_m/P_1 in the cross section 1 (x/X_o=0.64) at M=5 versus the calculated pressure ratio ξ in the oblique shock wave

The maximum values of Stanton number St_m and pressure coefficient Cp_m in the section x/X_o=0.64 at different fin angles are displayed in Fig. 6 as functions of ξ, where ξ is the pressure ratio behind the shock and in front of it at the non viscous flow. The value of St_m is normalized by the turbulent value of Stanton number calculated for the sharp plate in the same section. The heat transfer coefficient is measured by the "thin wall" sensors near the thickened fins (b = 37.5 mm); and the surface pressure is measured by PSP near the fins 25 mm in thickness. In the case of the sharp plate, the presented results are in agreement with data of Schulein [8]. The discrepancies are of approximately 15%. They are caused by: a) errors of measurements, b) small differences in the flow conditions (in

[8] the measurements were carried out at $x/X_o \geq 0.3$), c) different determination of the undisturbed values (in [8] St_o and P_1 were determined experimentally).

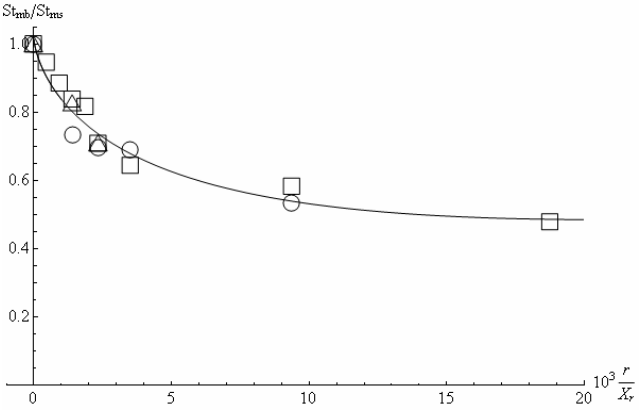

Figure 7: Maximum Stanton number in the cross section 1 (x/X_o=0.64) at M=5 versus the related bluntness radius: △ - θ = 10°, □ - θ = 15°, ○ - θ =20°

Fig. 7 demonstrates influence of the plate bluntness on the ratio St_m/St_{ms}. Here St_{ms} is the maximum value of the Stanton number on the sharp plate in the same section x/X_o=0.64. It is seen that at all the investigated fin angles, the plate blunting reduces the heat transfer near the fin in an equal degree. A significant reduction of heat transfer occurs at the increase of the plate bluntness radius only up to $r/X_o \approx 0.010 - 0.015$, i. e. at the turbulent state of the undisturbed boundary layer, the stabilization of the ratio St_m/St_{ms} occurs at smaller relative bluntness radius than at the laminar and transient states of boundary layer (0.02-0.03 [12,13]).

4.4 Comparison of the calculations results with the data

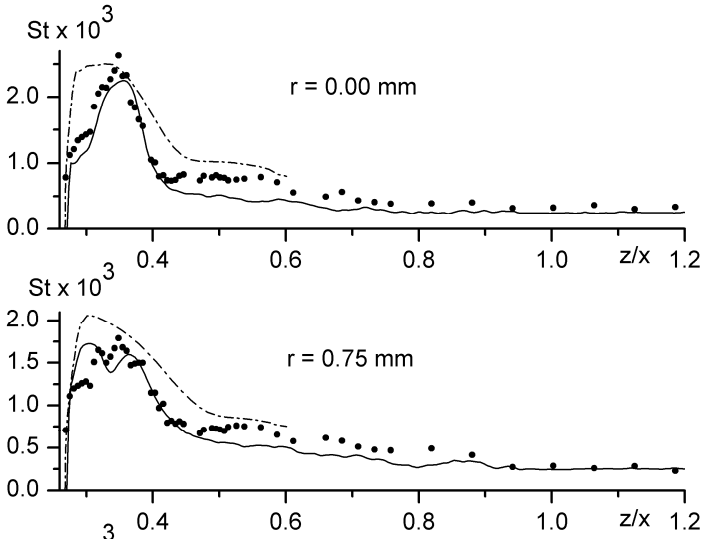

Figure 8: Stanton number distribution in the cross section 1 (X =211 mm, x/X_o = 0.64) at M=5, θ =15° : dashed lines – calculation, solid lines – TSP, points – thermocouples.

The calculated heat transfer distributions at M=5 on the plate near the fin with the angle θ=15° are compared with the experimental data in Fig. 8. The measurements are implemented by both the thermocouple sensors and the luminescent coating. In general, the calculation results satisfactorily comply with the experimental data. The predictions are closer to the data obtained by the thermocouple sensors which are more accurate than the results of optical measurements.

5. Fin pair on the plate

5.1 Flow patterns

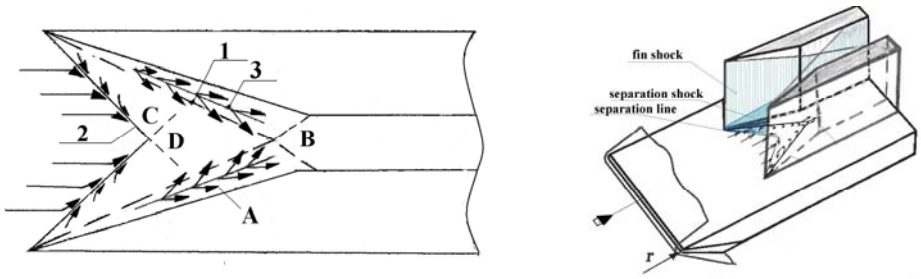

Figure 9: Regular flow pattern near a fin pair installed on a sharp or slightly blunted plate. 1 – fin shocks, 2 – separation lines, 3 – reattachment lines, A, B, C, D – areas of enhanced heat transfer

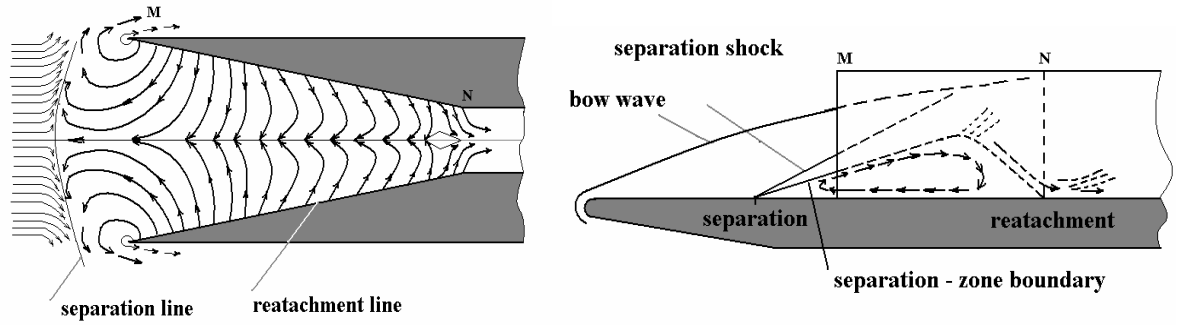

Figure 10: Non-regular flow pattern near a big-blunted plate.

The flow patterns near the fins, generating crossing shocks, are displayed in Figs. 9 and 10. Fig. 9 corresponds to the sharp plate. This case is investigated in details experimentally and numerically [7, 8]. The main shock waves 1, generated by the fins, cause boundary layer separation. The boundary layer separates on the lines 2 and reattaches near the fins, on the lines 3. The separation zones in turn generate the separation shocks. In contrast to the main shocks, the separation shocks are inclined not only to the undisturbed flow direction but also to the plate surface. The regions of amplified heat exchange and high pressure (regions A) are formed behind the shocks 1 (in the vicinity of the divergence lines 3), as in the case of a single fin. The region of even higher pressure and more intensive heat exchange (region B) is formed behind the intersection point of the main shocks. Behind the separation shocks (in the regions C), some increase of heat transfer and pressure takes place. Finally, one more region of intensive heat exchange (region D) is formed behind the intersection point of the separation shocks. The lines of secondary separation, which are not shown in Fig. 9, are generated inside each zone of separation.

The blunted leading edge of the plate generates an entropy layer. A part of this layer is involved into the separation flow near the fins. Due to the increase of mass, involved into the separation flow, the separation zones expand and the separation lines 2 displace forward, towards the undisturbed flow. Correspondingly, the oblique separation shocks displace forward, and the angle between them and the undisturbed flow direction increases. However at small bluntness, the regular flow with the plane separation shocks shown in Fig. 9 is kept.

At a certain bluntness value, a qualitative change of the flow occurs: two plane separation shocks merge in one curved separation shock; it is expelled forward and its origin is located in front of the fins (Fig. 10). The boundary layer separates also in front of the fins and reattaches partly near the fins (as in the case of the regular flow) and partly at the throat of the channel, formed between the fins. From the throat, one part of the separated gas moves back and the other one continue flowing in the normal direction.

The expected reason of the flow transformation consists in the following: at a sufficiently high inclination angle of the separation shocks (with respect to the undisturbed flow), the regular interaction of the separation shocks changes into the Mach interaction; it leads to formation of a strong shock and to generation a jet with reduced total pressure. At small throat width, this results in chocking of the near-wall part of the channel and to the expelling of the separation shocks.

The picture observed is similar to unstart of a convergent channel. However, there are significant differences: in the case of the unstart, the flow behind the expelled bow wave becomes subsonic, with the total pressure loss being sharply increased. In the considered case, the flow outside the separation zone even at the expelled separation shocks remains supersonic, and the total pressure losses are not so high as in the case of the unstart. In the case of unstart, the entire flow behind the channel leading edges transforms, and in the considered case, only the near-wall part of the channel flow significantly varies. However, the bluntness influence can be more significant if the fins are

situated between two plates: the blunting of the plates can cause unstart of the channel even at a relatively small contraction of the channel.

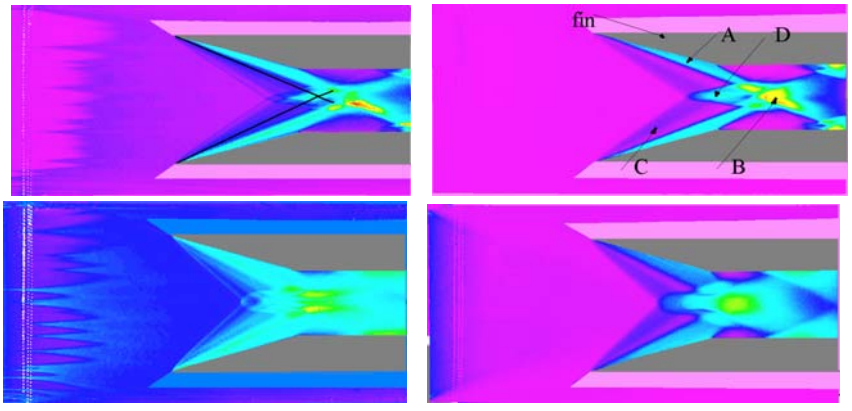

Stanton number Pressure coefficient

Figure 11: Flow fields near the fin pair at M = 5 and channel contraction ratio h/H =0.50.

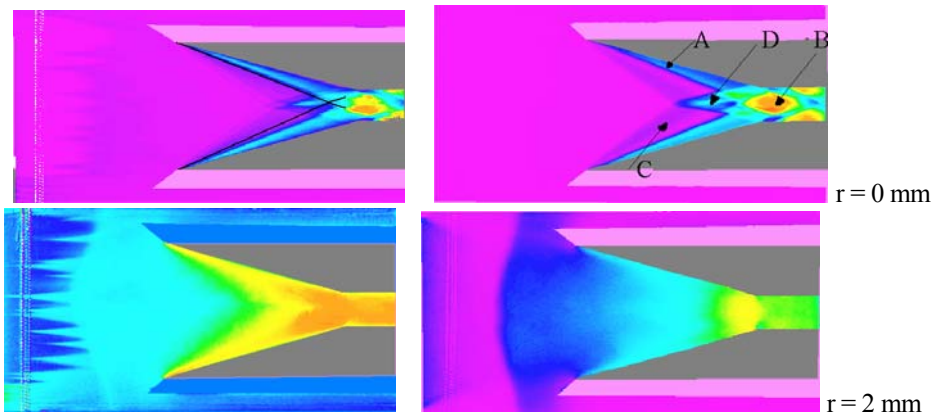

Stanton number Pressure coefficient

Figure 12: Flow fields near the fin pair at M = 5 and channel contraction ratio h/H =0.25.

The flow patterns presented in Figs. 9 and 10 are based on the data given below. The fields of Stanton number St and pressure coefficient C_P are displayed in Figs. 11 and 12 for the sharp and blunted plates at M=5 and $Re_{\infty L}$= $27x10^6$ in two cases: at the channel contraction ratio h/H = 0.5 and 0.25 (H =100 mm). In addition, the surface flow visualization and the schlieren-photos for the case h/H = 0.25 are presented in Fig. 13.

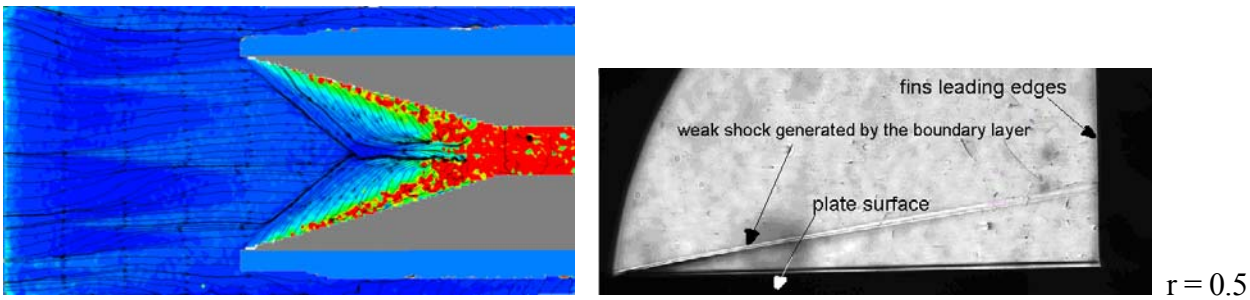

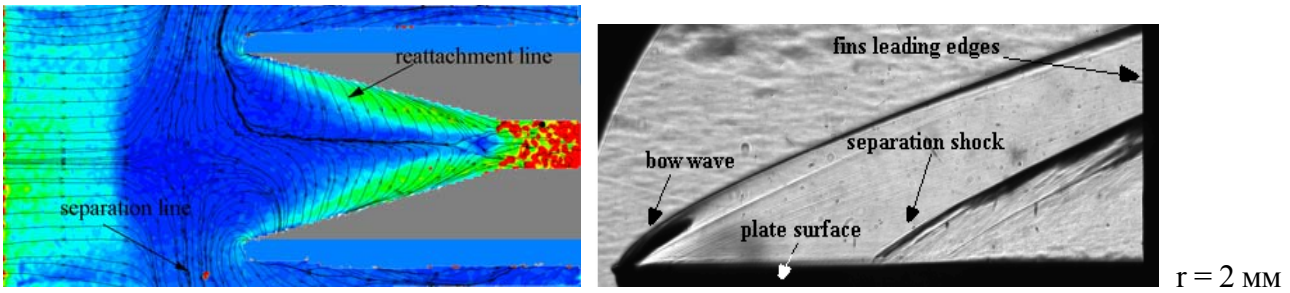

Figure 13: Limiting stream lines, skin friction and schlieren-photographs at M = 5 and channel contraction ratio h/H = 0.25.

At the small channel contraction (at h/H = 0.5, Fig. 11), the regular flow is seen on the sharp plate. Mach interference between the separation shocks can be supposed at the bluntness r =2 mm. But it does not result in shocks expelling at the contraction rate h/H = 0.5. The plate blunting reduces the heat exchange and pressure in the interference region. Simultaneously, it leads to expanding the regions of amplified heat exchange and increased pressure.

In the case of high channel contraction (at h/H = 0.25, Fig. 12), the behavior of the heat transfer coefficient distribution sharply changes at a certain value of the plate bluntness radius (in the considered case, at r = 2 mm). It is seen in Figs. 12 and 13 that at r = 2 mm, the separation line is formed in front of the fins. Behind it, the heat transfer and pressure coefficients increase, and the skin fiction decreases. High level of skin friction remains only behind the reattachment line (behind the channel throat). At the flow with expelled separation shocks, only one region of amplified heat exchange is observed, namely the region B. It is caused by formation of the divergence line and pressure peak at the end of separation zone. At r = 0.5 mm, only the bow wave generated by the blunted leading edge is seen in Fig. 13, because the main oblique shocks and the separation shocks are “hidden” by the fins. At r = 2 mm, it is possible to see in Fig. 13 the separation shock, too. Its inclination angle (about 30^o) corresponds to the high inclination angle of the separation-zone boundary (about 20^o at M=5) what is typical for the shock/turbulent-boundary-layer interaction.

Few experiments have been carried out at the same Mach number M=5 but at a reduced total pressure (P_t = 14 bar, $Re_{\infty L}=5.8x10^6$). In this case, the separation shocks are expelled already at the plate bluntness radius r = 0.75 mm. The inclination angle of the separation shock (about 20^o) corresponds to the relatively small inclination angle of the separation-zone boundary (10^o), as in the case of laminar flow. The bigger influence of the plate blunting at the reduced total pressure is connected with thickening the boundary layer and corresponding expansion of the separation zones.

5.2 Distribution of heat transfer and pressure coefficients in the interference zone

The distribution of Stanton number St (according to the sensors data) and pressure coefficient C_P (according to the PSP indications) in the section 1situated in front of the channel throat is presented in Fig. 14. The coordinate system shown in Fig. 1 is applied (the origin is situated near the fin leading edge). In the considered section, the fins interaction is noticeable only near the symmetry line, whose position is characterized by the ratio z/x = 0.61. In the remaining part of the section 1, the distributions of St and C_P at both contraction ratios h/H = 0.5 and 0.25 practically coincide within the range of the blunting radii from r = 0 up to r =0.5 mm (only the data for r =0 are given in Fig. 14 at h/H =0.5). Fig.14 demonstrates possibility two flow structures at r=0.75 mm: the regular flow (at the measurements of heat transfer coefficient, Fig. 14 a) and the flow with expelled separation shocks (at the pressure measurements, Fig. 14 b). The observed instability of the flow structure can be related both to some uncertainty of the test regime and to the difference in surface roughness and in its temperature. At the regular flow, the plate blunting reduces the heat exchange and decreases the degree of pressure rise.

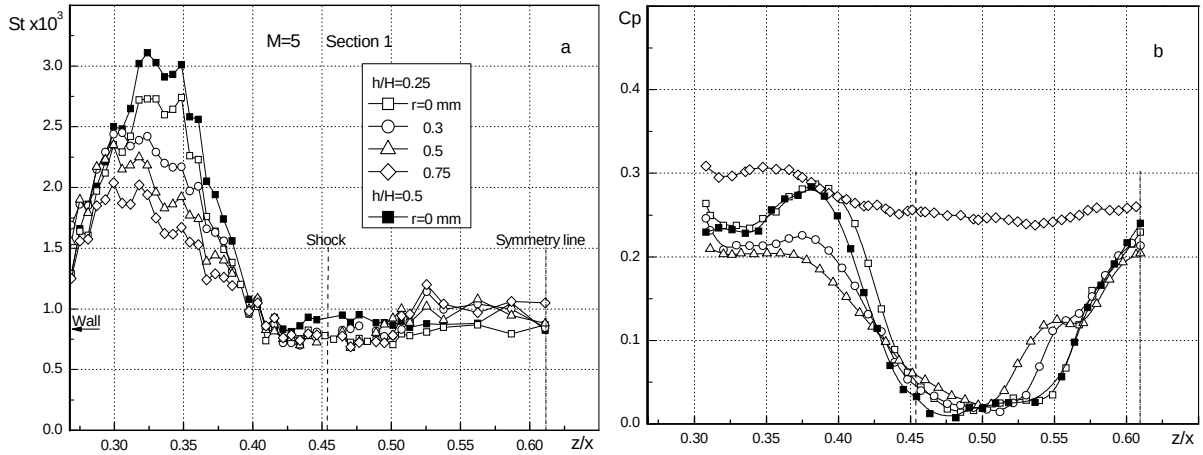

Figure 14: Stanton number and pressure coefficient distributions in the cross section 1 ($x/X_o = 0.64$) at M = 5.

The Stanton number distributions in the section 2 at high and small channel contractions are presented in Fig. 15. Here the lateral coordinate z is normalized by the channel width H. Unfortunately, the fins where installed at some angle relative the undisturbed flow direction (at about 50'). Therefore asymmetry of heat transfer distribution is observed. As the blunting radius increases, the heat exchange intensity in the section 2 significantly reduces as in the section 1. Simultaneously, the asymmetry of Stanton number distribution decreases.

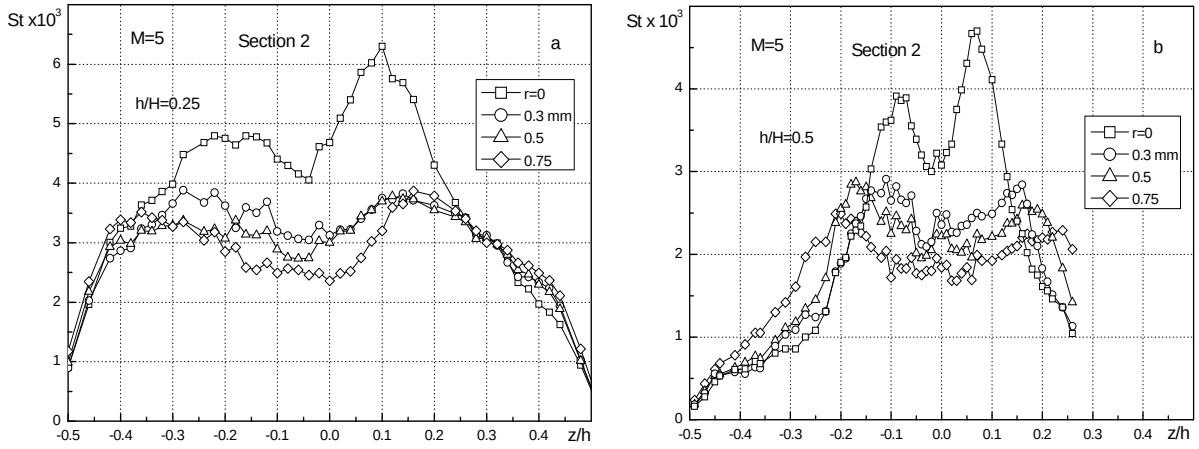

Figure 15: Stanton number distributions between the fins in the cross section 2 ($x/X_o = 1.1$) at big and small channel contractions (M=5, $Re_{\infty L} = 27x10^6$).

The maximum values of the heat transfer and pressure coefficients in the section 1 slightly depend on the channel contraction ratio. But in the section 2, situated behind the channel throat, St_m is approximately 1,5 times higher at h/H = 0.25 than at h/H = 0.50 due to the higher gas compression (Fig. 16,a). At the same time, the ratio St_m/St_{ms} in both sections depends in general only on the normalized blunting of the plate leading edge: the increase r/X_o from 0 up to $r/X_o \approx 0.015$ causes the decrease of Stanton number St_m by 50-60%, and the further increase r/X_o slightly influences the value of St_m (Fig.16,b).

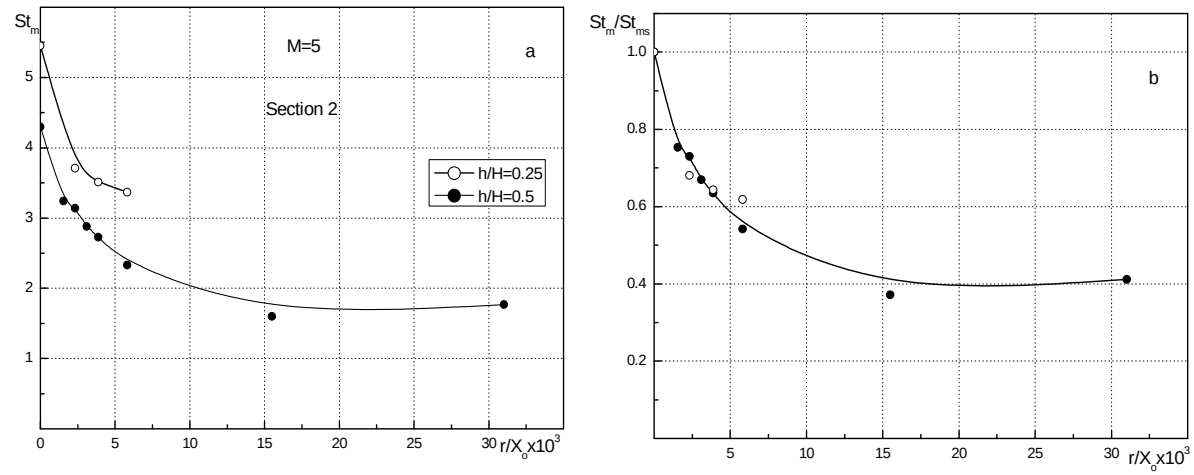

Figure 16: Maximum Stanton number in the cross section 2 versus the related plate bluntness at M = 5.

5.3 Influence of Mach number on the flow and heat exchange

The results, obtained at M=6, are similar to the presented above results for M=5. But at M = 6, the flow transformation occurs at a less blunting (r=0.75 mm) than at M=5 (r=2 mm) (both investigations are performed on the same model during heat transfer measurements).

The test results, obtained at M = 8, are presented in Figs. 17 – 19. At high channel contraction (at h/H = 0.25), even the small plate blunting r = 0.3 mm causes the flow transformation (Fig. 17). The inclination angle of the separation shock (12.7°) corresponds to the small inclination angle of the separation-zone boundary (7°), characteristic for the laminar flow. As the blunting radius increases up to r = 0.75 mm, appear signs of mixing-layer turbulization. At the same time, the inclination angles of the separation shock and the separation-zone boundary increase (up to 15.4° and 10° correspondigly).

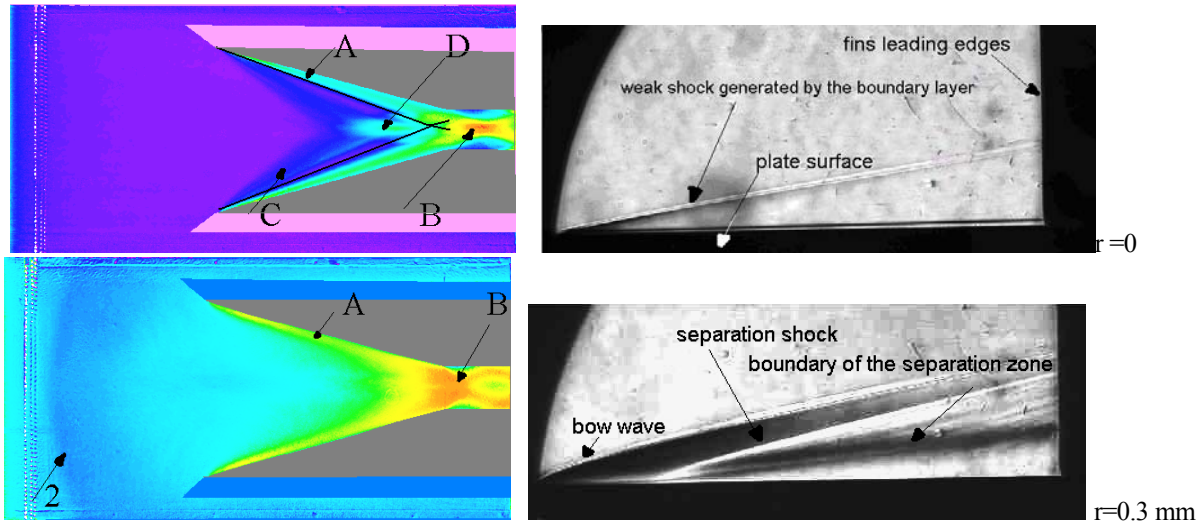

Figure 17: Flow fields at M = 8 and h/H =0.25.

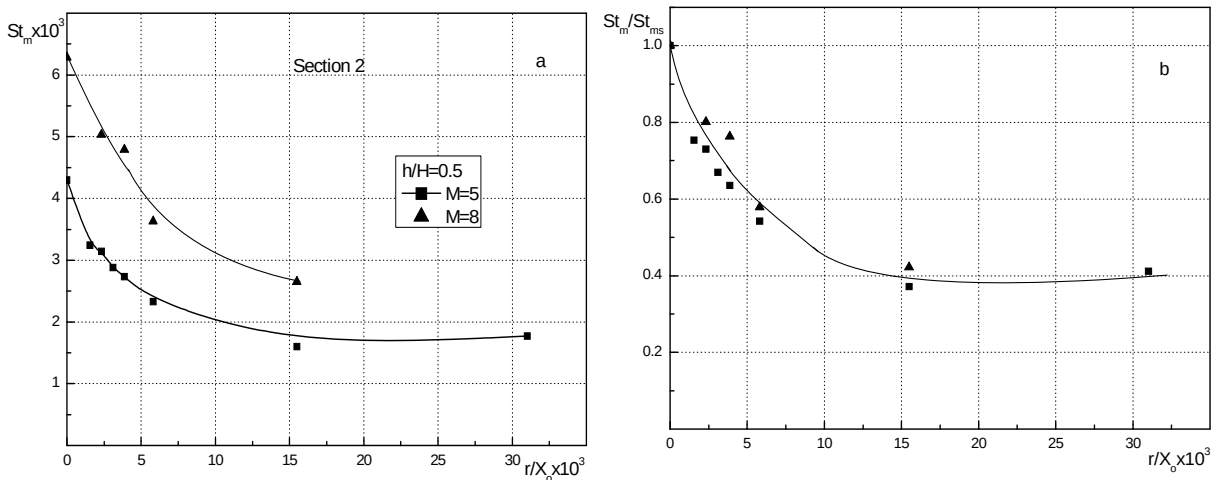

Figure 18. Maximum Stanton number in the cross section 2 versus the related plate bluntness at h/H = 0.5, M = 5 and 8.

Behind the channel throat, for example in the section 2, variation of the free flow Mach number in the investigated range slightly influences the degree of heat-transfer reducing (the ratio St_m/St_{ms}, Fig. 18,b). On the contrary, in front of the channel throat, the blunting influence on the heat transfer increases with increase of Mach number. The same is observed at the flow over a single fin and at a two-dimensional flow. Thus, the Mach number influences differently on the heat exchange in the interaction zone, depending on the flow type. This problem deserves further investigation.

Fig. 19 demonstrates the blunting influence on the maximum pressure in the sections 1 and 2 at M=8. It is seen that expelling of the separation shocks terminates the monotony of the pressure dependences versus the bluntness radius: after shocks expelling, the pressure drop in front of the channel throat (in the section 1) is changed into its increase, and behind the throat (in the section 2), the pressure drop stops.

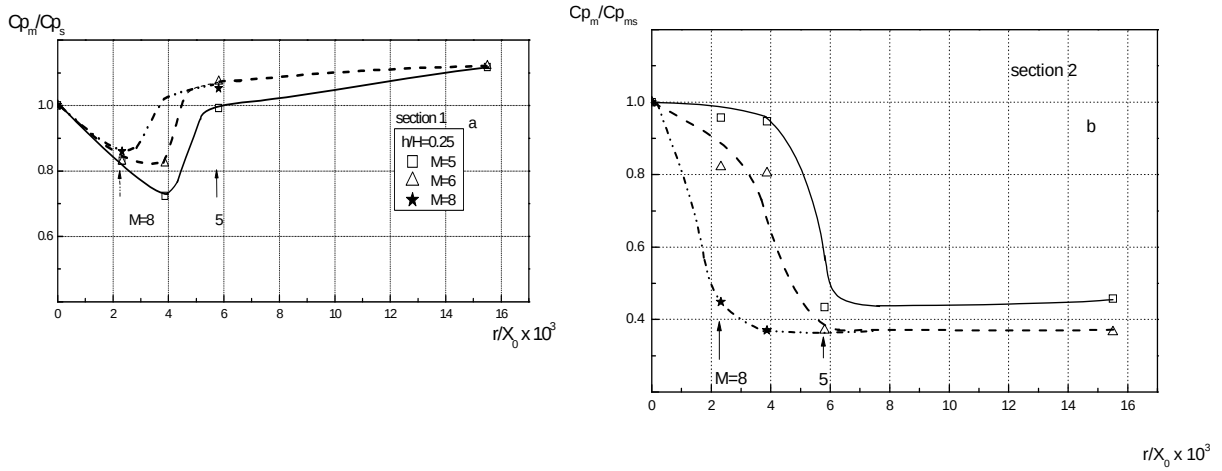

Figure 19. Maximum values of pressure coefficient in the cross sections 1 and 2 versus the related plate bluntness at M = 5 , 6 and 8. The arrows denote the flow transformation.

Conclusions

The surface flow and heat exchange on the sharp and blunted plates in the presence of a fin or a fin pair, generating crossing shocks, are investigated at Mach numbers M=5, 6, and 8 and Reynolds numbers up to $Re_{\infty L}=27x10^6$. There was shown that the entropy layer, generated by the small blunting of the plate leading edge, significantly changes the heat transfer, pressure, and skin friction in the region of shock-wave/boundary-layer interaction, and at some conditions, it can cause transformation of the flow structure. In particular, the following was established.

At overflow of a single fin, the separation zone is formed with the reattachment line situated at the fin. Near the fin leading edge (in the initial region), the values of heat transfer and pressure coefficients on the reattachment line increase gradually with the downstream distance from the fin leading edge. They achieve the maximum values St_m and Cp_m only at a significant distance from the fin leading edge (in the region of quasi-conical flow). As the blunting rises, the length of the initial region increases.

The maximum values of heat transfer and pressure coefficients (St_m and Cp_m) near the single fin decrease as the blunting radius of the plate leading edge increases. Simultaneously expands the region of amplified heat exchange

and increased pressure. At a certain value of relative blunting radius r/X_o, significant change of St_m and Cp_m terminates. The described influence of the plate blunting on the gas flow is observed at all the investigated fin angles. It amplifies as the Mach number increases.
Results of numerical calculation of the Stanton number distribution near a single fin, implemented using the q-ω turbulence model, satisfactorily comply with the experimental data.
In the case of a fin pair, generating crossing shocks, the heat exchange and pressure behind the intersecting shocks significantly increase as compared to the case of a single fin. As the contraction degree of the channel formed between the fins rises, the maximum heat transfer and pressure coefficients behind the crossing shocks increase.
At high channel contraction, the separation shocks are expelled from the channel towards the undisturbed flow when the plate blunting radius exceeds a certain critical value. At that, instead of two narrow separation zones situated near the fins, one vast separation zone is formed. It begins in front of the fins at a great distance from them and terminates at the channel throat. The flow transformation changes the heat transfer and pressure distributions both in front of the fins and between them. The critical blunting value decreases as the Mach number increases.
As in the case of a singe fin, the increase in the plate blunting radius within a certain range (up to $r/X_o \approx 0.015$) significantly reduces heat transfer and pressure in the interaction region, if the regular flow (i. e. without expelling the separation shocks) is kept.

The research was supported by International Science and Technology Center (ISTC) under Grant #3872 and Russian Foundation for Basic Researches (RFBR) under Grants No. 08-01-00449 and 11-01-00657.

References

1. *Miller D.S., Hijman R., Redeker E., Janssen W.C., Mullen C.R.* A study of shock impingement on boundary layer at Mach 16 // Heat Transfer and Fluid Mechanics Institute. Stanford, Calif.: Univ. Press, 1962. P. 255 - 278
2. *Borovoy V.Ya., Sevastyanova E.V.* Gas flow and heat exchange in the region of interaction of a laminar boundary layer with the shock wave near a half-wing, installed on the plate // Uchenye zapiski TsAGI. 1973. V. 4. Issue 2. pp. 54 - 63.
3. *Zheltovodov A.A.* Physical peculiarities and some features of two-dimensional and three-dimensional flows with separation at supersonic velocities // Izvestiya Rossiskoi Academii Nauk, Mekhanika Zhidkosti I Gaza. 1979. Issue 3. pp. 42 - 50.
4. Knight D.D., Horstman C.C., Shapey B., Bogdonov S. Structure of supersonic turbulent flow past a sharp fin. // AIAA Journal. 1987. V. 25. No.10. P. 1331 - 1337.
5. Kussoy M.I., Horstman K.C., Horstman C.C. Hypersonic crossing shock-wave/turbulent-boundary-layer interactions. AIAA Journal. V. 31. No.12. 1993. Pp. 2197-2203.
6. Garrison T.J., Settles G.S., Narayanswami N., Knight D.D. Structure of crossing-shock-wave/turbulent-boundary-layer interactions. AIAA Journal. V. 31. No.12. 1993. Pp. 2204-2211.
7. Knight D., Yan H., Panaras A.G., Zheltovodov A. Advances in CFD prediction of shock wave turbulent boundary layer interactions // Progr. in Aerospace Sci. 2003. V. 39. No. 2-3. P. 121 - 184.
8. *Schulein E.* Skin-friction and heat flux measurements in shock/boundary-layer interaction flows // AIAA Journal. 2006. V. 44. No. 8. P. 1732 - 1741.
9. *Borovoy V. Ya., Egorov I. V., Skuratov A. S., Struminskaya I. V.* Interference of an oblique shock with the boundary and high entropy layers of the flat plate. Izvestiya Rossiskoi Academii Nauk, Mekhanika Zhidkosti I Gaza. 2005. Vol.40. No. 6. Pp. 89 - 108.
10. *Borovoy V.Ya., Skuratov A. S., Struminskaya I. V.* On the existence of a threshold value of the plate bluntness in the interference of an oblique shock with boundary and entropy layers. Izvestiya Rossiskoi Academii Nauk, Mekhanika Zhidkosti I Gaza. 2008. Vol.43. No. 3. Pp. 41 - 52.
11. *Borovoy V. Ya., Egorov I. V., Skuratov A. S., Struminskaya I. V.* Two-dimensional interaction of the oblique shock wave with the boundary and high-entropy layers of the blunt plate. AIAA 2011-731. 2011.
12. *Borovoy V. Mosharov V., Radchenko V., and Noev A.* Laminar-turbulent flow around a fin placed on sharp and blunted plates. EUCASS 2009.
13. *Borovoy V.Ya. Mosharov V.E., Radchenko V.N., and Noev A.Yu.* Laminar-turbulent flow around a fin placed on sharp and blunted plates. Izvestiya Rossiskoi Academii Nauk, Mekhanika Zhidkosti I Gaza. 2009. Vol.44. No. 3. pp. 58 - 74.